



# Self-power electroreduction of N<sub>2</sub> into NH<sub>3</sub> by 3D printed triboelectric nanogenerators

Shuyan Gao<sup>1,\*</sup>, Yingzheng Zhu<sup>1</sup>, Ye Chen<sup>1</sup>, Miao Tian<sup>1</sup>, Yingjie Yang<sup>1</sup>, Tao Jiang<sup>2</sup>, Zhong Lin Wang<sup>2,3,\*</sup>

<sup>1</sup> School of Chemistry and Chemical Engineering, Henan Normal University, Xinxiang, Henan 453007, PR China

<sup>2</sup> Beijing Institute of Nanoenergy and Nanosystems, Chinese Academy of Sciences, Beijing 100083, PR China

<sup>3</sup> School of Materials Science and Engineering, Georgia Institute of Technology, Atlanta, GA 30332-0245, USA

Conversion of naturally abundant nitrogen (N<sub>2</sub>) into ammonia (NH<sub>3</sub>) is a vital (bio)chemical process to sustainable life, and it remains as a grand challenge in chemistry and biology. Although electrocatalytic nitrogen reduction reaction (NRR) provides an intriguing blueprint for the sustainable conversion of N<sub>2</sub> into NH<sub>3</sub> by sidestepping the hydrogen- and energy-intensive operations of the Haber–Bosch process, it is severely challenged by (1) the continuous energy supply consumption deriving from fossil fuels and (2) the dependence on metal-based catalysts for the nitrogen activation and reduction reaction. From energy- and resource-saving perspectives, self-powered NRR system with metal-free electrocatalysts is strongly desired. Herein, we tacitly integrate 3D printing technology with personalized fabrication of printed triboelectric nanogenerators (TENGs) for self-powered NRR. The printed TENGs produce an output power density from 1.48 to 6.7 W m<sup>-2</sup> and the assembled self-powered N<sub>2</sub> fixation system could reach NH<sub>3</sub> yield of 36.41 μg h<sup>-1</sup> mg<sub>cat.</sub><sup>-1</sup>, representing a pioneering step toward perfect marriage of digital manufactured TENGs by 3D printing with self-powered sustainable metal-free NRR under ambient conditions. The present work highlights various accesses to the flexible, shape-adaptive, personalized, energy-/resource-saving integration of 3D-printed TENGs with metal-free electrocatalysts to self-power N<sub>2</sub> fixation.

## Introduction

Fixation of naturally rich nitrogen (N<sub>2</sub>) into ammonia (NH<sub>3</sub>) has a significant effect on the manufacturing of nitrogen fertilizers and alternative hydrogen-rich fuels, leading to fundamental changes in the way food is produced and improving energy production and environmental sustainability to eliminate hunger and sustaining all life forms [1–3]. Although molecular N<sub>2</sub> in the atmosphere is widely available (78% in the atmosphere), the highly stable N≡N covalent triple bond with the bond

energy of 940.95 kJ mol<sup>-1</sup> makes N<sub>2</sub> fixation under mild conditions a great challenge [4–6]. As such, harsh conditions of Haber–Bosch process (high pressure >150 bar and temperature >450 °C) are demanded to convert N<sub>2</sub> to available nitrogen-containing compounds such as NH<sub>3</sub>, resulting in 1–2% of the world's annual energy supply consumption deriving from fossil fuels [4,6,7]. Even electrochemical reduction of N<sub>2</sub> into NH<sub>3</sub> offers a promising carbon-free strategy toward greener NH<sub>3</sub> production [8–12], self-powered sustainable fixation methods for NH<sub>3</sub> from N<sub>2</sub> together with metal-free electrocatalysts are strongly desired from energy- and resource-saving perspectives to totally sidestep the energy supply consumption deriving from fossil fuels and metal-based mainstream electrocatalysts.

\* Corresponding authors at: School of Chemistry and Chemical Engineering, Henan Normal University, Xinxiang, Henan 453007, PR China (S. Gao); School of Materials Science and Engineering, Georgia Institute of Technology, Atlanta, GA 30332-0245, USA (L. Wang).

E-mail addresses: Gao, S. (shuyangao@htu.cn), Wang, Z.L. (zhong.wang@mse.gatech.edu).

Triboelectric nanogenerator (TENG), as a burgeoning energy harvesting technology, can convert mechanical energy from the environment into electric energy, and it has become one of the most significant inventions in energy harvesting technologies. The integrated self-powered systems have already successfully harvesting human motion energy [13], vibration energy [14–17], wind energy [18–20], flowing water [21–23], raindrops [24,25], even the large-scale blue energy [24–28], and been innovatively applied in electrochemical applications, portable/wearable personal electronics, biomedical monitoring, nanorobotics, micro-electromechanical systems and so on. With the increasing demands and special individual customized needs for self-powered energy sources in these high-tech fields, individualized design and flexible manufacturing are the best choice, avoiding the disadvantages of traditional manufacturing methods, such as requiring professional forming mold. 3D printing, as the state-of-the-art and highly efficient additive manufacturing technology, has recently developed at an impressive pace and played an irreplaceable role in many fields such as tissue engineering [29–31], soft robotics [32–35], optical engineering [36–38], electronic devices [39,40], energy storage and energy harvesting/conversion devices [41–44], and so on. The excellent integration with computer-aided design software makes 3D printing technology theoretically realize the construction of any complicated structure from the nanoscale to macroscale in a printable manner to meet customized demands [45]. 3D printing is considered as not only the key technology for green and intelligent development of the future high-end equipment but also the core technology for the third industrial revolution. The era of 3D printing will come inexorably with the constantly deepening integration of 3D printing technology and innovative design.

In order to accelerate the innovative development and deepen application of self-powered systems with TENG as the driving source, we herein take the advantages of 3D printing technology to fabricate TENGs endowed with excellent output characteristics, cost-effectiveness, flexible configuration, individual geometry structure, simplicity to make, and so on. Three kinds of TENGs with different structures were manufactured by 3D printer utilizing soft material of thermoplastic elastomer (TPE) filament and hard material of polylactic acid (PLA) filament as the consumables. These three kinds of TENGs include a printed elastic triboelectric nanogenerator (PE-TENG) with four elastic folding units manufactured with soft material of TPE, and a series of printed multi-layer linkage TENG (PMLL-TENG) with different outline of friction layers as well as a printed multi-layer asway triboelectric nanogenerator (PMLA-TENG) with hard material of PLA. As to these printed TENGs, the complexity of geometry structure upgrades gradually from simple to complex. Their open-circuit voltage ( $V_{oc}$ ) ranges from 410 to 2360 V, short-circuit current ( $I_{sc}$ ) spans from 420  $\mu$ A to 1.7 mA, and the output power density increases from 1.48 to 6.7 W m<sup>-2</sup>. Such performances qualify these TENGs as promising power sources *via* harvesting mechanical energy from various ambient environments, as pioneered here to electrochemically fix N<sub>2</sub> into NH<sub>3</sub> self-powered by PMLA-TENG, where melamine-sponge-based carbon materials, prepared using melamine sponge (MS) as precursor and named as MSCM, are utilized as cathode catalyst. With a working frequency of 10 Hz, such assembled self-powered N<sub>2</sub> fix-

ation system could reach NH<sub>3</sub> yield of 36.41  $\mu$ g h<sup>-1</sup> mg<sub>cat.</sub><sup>-1</sup>, indicating its high-performance for electrochemical synthesis of NH<sub>3</sub> at ambient conditions. Systematical study on a series of control experiments demonstrates that N<sub>2</sub> can be directly reduced at the cathode interface self-powered by PMLA-TENG. Integrated with the compelling features, such as flexible design and wide availability of TENG, high synthetic efficiency for NH<sub>3</sub>, and metal-free cathode catalyst, the present work provides various accesses to other 3D-printed self-powered N<sub>2</sub> fixation system with flexible, shape-adaptive, energy-/cost-saving integration to achieve an ambitious breakthrough and open up a new road in the synthetic ammonia industry toward a lower-energy and more sustainable process.

## Material and methods

### *The overall structure design and fabrication of TENGs*

The 2D rough sketch for the structure design of TENGs were drawn by software of Auto CAD (Autodesk, Inc.), then 3D modeling, simulating assembly, motion simulation were all finished in software of Solidworks (Dassault Systemes S.A). The corresponding potential distribution was simulated by COMSOL (COMSOL Inc.). The 3D model files were imported into software of Cura (Ultimaker) to slice and obtain the gcode files to drive FDM printer. After loading the gcode files into the FDM printer (Hue Way 3D-160), soft and hard filament consumables were extruded through a heated nozzle of the 3D printer to melt, deposit and fuse the material.

For the first kind of 3D printed TENG, PE-TENG, the supporting substrate included four flexible folding units and each unit provided six frictional contact layers. And then twenty-four thin copper foils with size of 40 mm  $\times$  18 mm  $\times$  110  $\mu$ m were pasted on the substrate as the metal electrode and friction layer. Twenty-four pieces of PTFE films with size of 40 mm  $\times$  18 mm  $\times$  50  $\mu$ m attached onto another twenty-four pieces of thin copper foil with size of 40 mm  $\times$  18 mm  $\times$  50  $\mu$ m, and then attached to substrate and made the surface of the PTFE face metal electrode. For PMLL-TENG, six thin copper foils with size of 100 mm  $\times$  90 mm  $\times$  110  $\mu$ m were pasted on the substrates as the metal electrode and friction layer. Six additional copper foils with size of 100 mm  $\times$  90 mm  $\times$  110  $\mu$ m as the back electrodes which were also adhered onto the substrates, and then six pieces of PTFE films with size of 100 mm  $\times$  90 mm  $\times$  110  $\mu$ m were pasted to the surface of back electrodes, and the surface of the PTFE films and the corresponding surface of the metal friction layers were face to face. There were three pairs of friction layers could contact simultaneously when an external reciprocating force applied to PMLL-TENG. For the sake of improving the surface charge density of PTFE films, all the PTFE films were handled by the charge injection method of high voltage corona charging. Twelve thin copper foils with size of 60 mm  $\times$  90 mm  $\times$  110  $\mu$ m in size were posted on the sponge with the same size respectively, which were adhered on the circumferential array asway substrate as buffers. The other twelve copper foils with the size of 60 mm  $\times$  90 mm  $\times$  110  $\mu$ m were glued on the fixed circumferential array substrate as the back electrode, and then twelve PTFE films with size of 60 mm  $\times$  90 mm  $\times$  50  $\mu$ m were pasted to the surface of copper foils. The two substrates were bolted to the

end cover specially designed and equipped with bearings. The end of connecting rod of the crank-rocker mechanism was connected to the circumferential array asway substrate, and the other end is connected to crank linked with a fan through a coupling shaft.

### Self-powered electrochemical $N_2$ fixation

Electrochemical reduction of  $N_2$  to  $NH_3$  was performed in an H-cell equipment with Nafion 117 membrane for separation. Before use, Nafion membrane was protonated by first boiling in DI water for 1 h, then treating in  $H_2O_2$  for 1 h and in DI water for another hour, followed by 3 h in  $0.5 \text{ mol L}^{-1} H_2SO_4$ , and finally for 6 h in DI water. All above steps were handled at  $80 \text{ }^\circ\text{C}$ . Self-powered electrochemistry was measured with PMLA-TENG as the power source, using a MSCM covered carbon paper as working electrode and a graphite rod as counter one. All experiments were performed at room temperature under atmospheric pressure. For  $N_2$  reduction experiments, the electrolyte ( $0.1 \text{ mol L}^{-1} HCl$  solution) was purged with  $N_2$  for at least 0.5 h before measurement. Pure  $N_2$  was uninterruptedly fed into the cathode during the experiments.

## Results and discussion

The first kind of TENG manufactured by a FDM 3D printer was PE-TENG with four flexible folding units using TPE filaments. The basic structure and fabrication process are shown in Fig. 1a, and the detailed assembly process is exhibited in the Experimental Section. Its digital image is shown in Fig. 1b. In order to exhibit the high deformability and excellent ability of reversible rehabilitation, the bent PE-TENG is shown in Fig. 1c. The extruded filamentous TPE with a length of 5 mm could even be stretched to 25 mm (Fig. 1d). TPE features a considerable elastic regime via physical crosslinks, which makes the elastic substrate have exotic mechanical behaviors, e.g., lightweight, high deformability and excellent ability of reversible rehabilitation [46,47]. With the coupling of triboelectrification and electrostatic induction, electricity was generated as illustrated in Fig. 1e. When external force applied, PTFE film fully contacted with the copper foil, triboelectric charges were released and transferred from copper to PTFE (i). When the external force unloaded, a potential difference was produced to drive the electrons from the back electrode to copper electrode, and an instantaneous negative current could be detected (ii). As the two surfaces completely separated, the inductive electrons and positive triboelectric charges were almost balanced (iii). When the external force loaded again, potential difference in opposite direction was generated, the inductive electrons were driven to back electrode in an opposite direction and an instantaneous positive current could be detected (iv) until the copper electrode and the PTFE film fully contacted again (i), and a new balance can be reached. The electricity generation process could be theoretically simulated by COMSOL (Fig. 1f). Moreover, a series of complicated structure with the similar elastic supporting substrates are also manufactured and exhibit in Fig. 2g.

Fig. 1h–m illustrate the output characteristics of the PE-TENG measured at the working frequency of 2–5 Hz. Along with the increase of friction unit, the  $I_{sc}$  and transferred charge ( $Q_{tr}$ )

increased from 100 to  $420 \mu\text{A}$  (Fig. 1h) and  $0.75\text{--}2.83 \mu\text{C}$  (Fig. 1i), while the  $V_{oc}$  ( $410 \text{ V}$ ) was nearly independent of the friction unit due to all the friction layers connected in parallel (Fig. 1j), consistent with previous findings [48,49]. In order to measure the output power of this PE-TENG, resistors from  $10 \Omega$  to  $1 \text{ G}\Omega$  were connected as external loads. As shown in Fig. 1k, with the increasing load resistance, the instantaneous current dropped and the instantaneous power density of the circuit reached a maximum value of  $1.48 \text{ W m}^{-2}$  when the resistance value was  $1 \text{ M}\Omega$ . The rectified  $I_{sc}$  ( $410 \mu\text{A}$ ) is exhibited in Fig. 1l, and the  $I_{sc}$  could reach 1 mA after regulated by a transformer (Fig. 1m). 100 commercial LED bulbs can be directly driven by PE-TENG (Fig. S1 and Movie S1), confirming its ability to capture mechanical energy from surrounding environment and behavior as a portable power source. This PE-TENG is a good example that 3D printing technique based on FDM integrating with soft material could be successfully applied in fabricating TENG devices characteristic of personalized and complicated structure, excellent output performance, exotic mechanical and durable character, and the advantages of lightweight, low manufacture cost, rapid prototyping, short fabricating period, etc.

In order to demonstrate the superiority of 3D printing technique in fabricating TENGs with more complex assembly structure, a series of novel TENGs, PMLL-TENG, were designed and fabricated using hard material of solid PLA filaments as the 3D printer's consumables. PLA with good mechanical and physical properties were environment friendly and biodegradable consumables, which could be printed easily without any hazard of air contamination and the problem of warping [50,51]. The basic structure and the fabricated process of one printed PMLL-TENG is exhibited in Fig. 2a. The detailed assembly process is explained in the experimental section. The potential distribution can be simulated by COMSOL (Fig. 2b). Another three PMLL-TENGs with different shapes of friction layers, ladder, arc, triangular are shown in Fig. 2c respectively. The effective friction contact area of these four structures gradually increases. Their output performance is exhibited in Fig. 2d–g. With the increase of effective contact area of the friction layer of different structures,  $I_{sc}$ ,  $V_{oc}$  and  $Q_{tr}$  slightly increased at the working frequency of 2–5 Hz. The  $I_{sc}$  was 0.52, 0.60, 0.60, 0.67 mA for these four PMLL-TENGs, respectively (Fig. 2d), their  $V_{oc}$  reached 1860, 1900, 2230, 2360 V, respectively (Fig. 2e), the  $Q_{tr}$  was measured to be 2.0, 2.2, 2.3, 2.5  $\mu\text{C}$ , respectively (Fig. 2f). Load resistances from  $10 \Omega$  to  $1 \text{ G}\Omega$  are also connected to each PMLL-TENG, and the instantaneous current decreases with increasing load resistance. When the load is  $1 \text{ M}\Omega$ , the instantaneous output power of PMLL-TENG with planar and trapezoidal profiles reaches the maximum value of 2.48 and  $2.84 \text{ W m}^{-2}$ , respectively. When the load is  $2 \text{ M}\Omega$ , the instantaneous output power of PMLL-TENG with planar and trapezoidal profiles reaches the maximum value of 3.15 and  $3.58 \text{ W m}^{-2}$ , respectively (Fig. 2g). Fig. S2 and Movie S2 show that the PMLL-TENG directly drove 250 commercial LED bulbs, proving that the PMLL-TENG had the capability as a power source that could harvest mechanical energy and convert into electricity. Finely handling different shapes of friction contact surfaces to increase the effective contact area of friction layer in finite space, this kind of PMLL-TENGs demonstrated the unique advantages of 3D printing technology in manufactur-

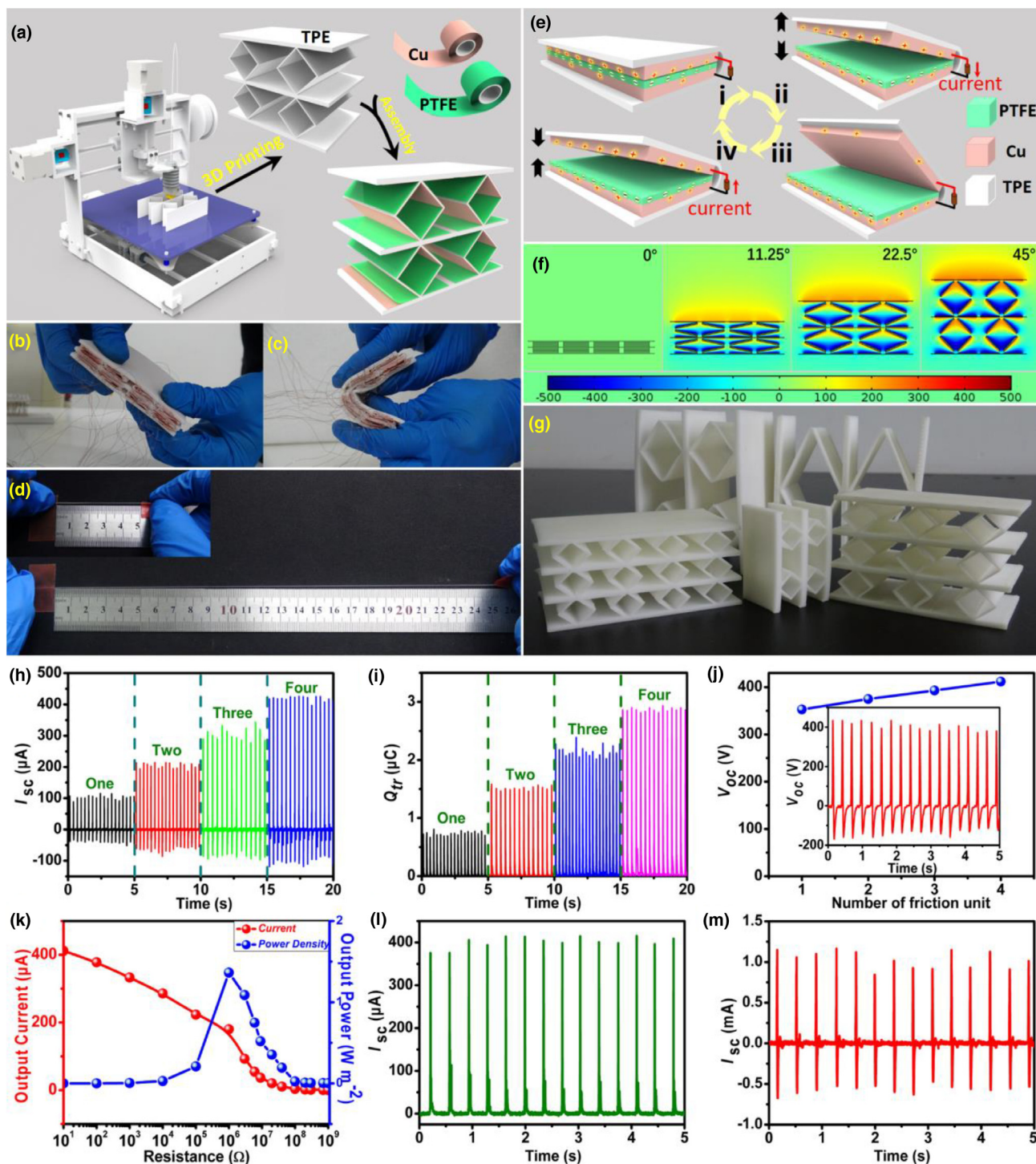


FIGURE 1

(a) Basic structure and fabrication process of the PE-TENG with four folding units. (b) Digital image of the PE-TENG with four folding units. (c) Digital image of the bent PE-TENG. (d) Tensile properties of the extruded filamentous TPE. (e) An illustration of an electricity-generating process of PE-TENG. (f) The potential distribution simulated by COMSOL with the angle changes. (g) Digital image of the other elastic supporting substrates of PE-TENG. (h)  $I_{sc}$ , (i)  $Q_{tr}$ , and (j)  $V_{oc}$  of the PE-TENG with different folding unit numbers.  $V_{oc}$  of the PE-TENG with four folding units is insetted in (j). (k) The instantaneous current and the power density of the PMLA-TENG with twelve friction layers as the load resistance increases. (l) The rectified  $I_{sc}$ . (m)  $I_{sc}$  after processed by a transformer.

ing personalized structural components with complex curve surface, showing the potential prospect in the deep combination of 3D printing technology with TENGs.

In order to testify the manufacturing and assembly accuracy, PMLA-TENG was manufactured by a FDM 3D printer with hard

material of PLA filaments. Fig. 3a show the fabrication process and basic structure of the PMLA-TENG. A crank-rocker mechanism was introduced to convert the rotating mechanical energy into swinging mechanical energy. The potential field distribution at different position were simulated by COMSOL (Fig. 3b).

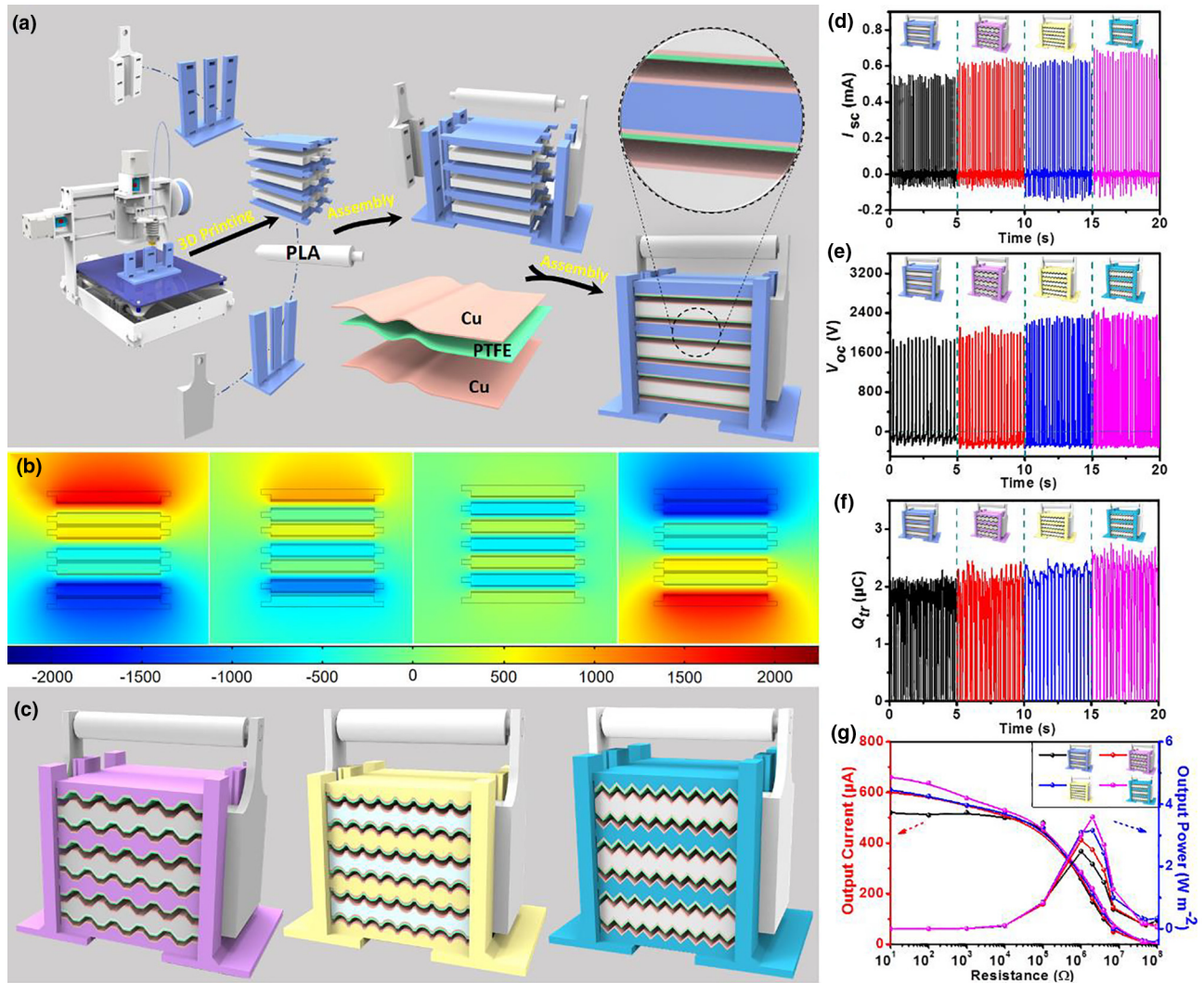


**FIGURE 2**

(a) Basic structure and assembly process of one PMLL-TENG with flat friction layer. (b) The potential distribution of the PMLL-TENG with flat friction layers simulated by COMSOL. (c) The other three PMLL-TENG with ladder, arc, triangular friction layers. (d)  $I_{sc}$ , (e)  $V_{oc}$ , and (f)  $Q_{tr}$  of the PMLL-TENGs with three fraction layers contact simultaneously. (g) The instantaneous current and the power density of the PMLL-TENGs with three fraction layers contact simultaneously as the load resistance increases.

The output performance at working frequency of 2–5 Hz is exhibited in Fig. 3c–h. A rotational external force was applied to drive the crank mechanism to realize the rocker mechanism swing, which made the swingable circumferential substrate contact with the fixed circumferential substrate and six fraction layers contacted at the same time. The output  $I_{sc}$  and  $Q_{tr}$  of the PMLA-TENG with different fraction layer are shown in Fig. 3c and d respectively. It is obviously that the output  $I_{sc}$  and  $Q_{tr}$  increase with the number of fraction layers from 300 to 1700  $\mu\text{A}$ , and from 0.58 to 2.58  $\mu\text{C}$ , respectively. The  $V_{oc}$  of the PMLA-TENG with different fraction layer is exhibited in Fig. 3e, and it has just little improvement because the electrode of every fraction layer is parallel and the maximum instantaneous  $V_{oc}$  can reach 1900 V. When connecting resistance from 10  $\Omega$  to 1 G $\Omega$ , its instantaneous current drops and the maximum instantaneous power density reaches 6.7  $\text{W m}^{-2}$  when the resistance value is 1 M $\Omega$  (Fig. 3f). The  $I_{sc}$  can reach 5.7 mA after processed by a transformer and a rectifier (Fig. 3g). After working continuously for

6 h (about 136,800 cycles), its  $I_{sc}$  processed by a transformer and a rectifier is still maintained at 5.7 mA, which is exhibited in Fig. 3h. Fig. S3 and Movie S3 show that the PMLA-TENG directly drove 250 commercial LED bulbs, testifying that the PMLA-TENG had the capability as a power source. The application of crank-rocker mechanism required high machining accuracy and assembly accuracy, which herein undoubtedly verified the unique advantages of 3D printing technology to introduce crank rocker mechanism into effective collection of rotational mechanical energy for TENG to realize harvesting the disorderly mechanical energy in the surrounding environment, such as wind energy, water kinetic energy and potential energy into the continuous circular motion of the crank to drive the TENG to generate electricity.

As discussed above, these printed TENGs feature with the geometry topology from simple plane to complex curved surface,  $V_{oc}$  from 410 to 2360 V,  $I_{sc}$  from 420  $\mu\text{A}$  to 1.7 mA, and the output power density from 1.48 to 6.7  $\text{W m}^{-2}$ , which qualify

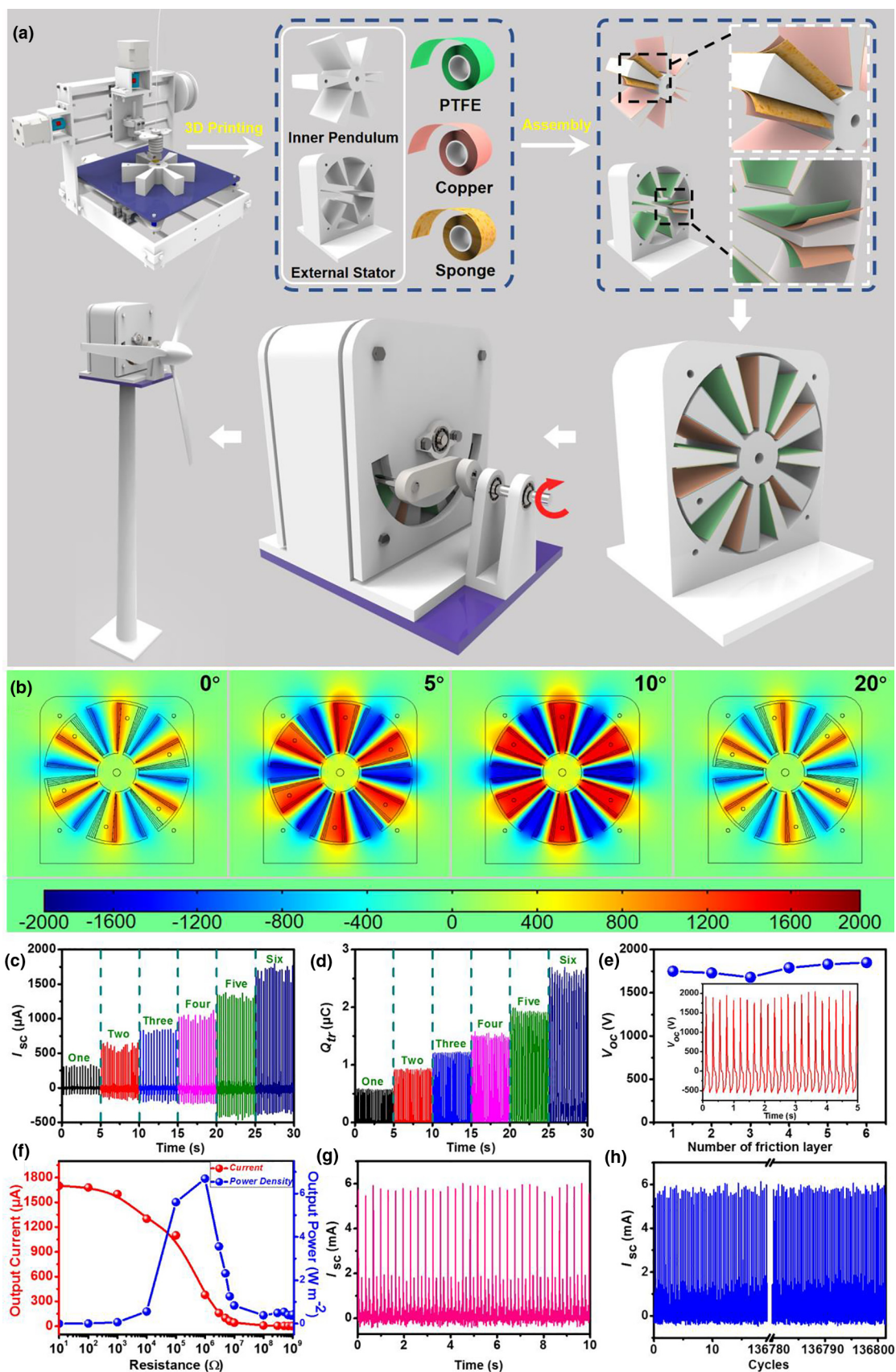
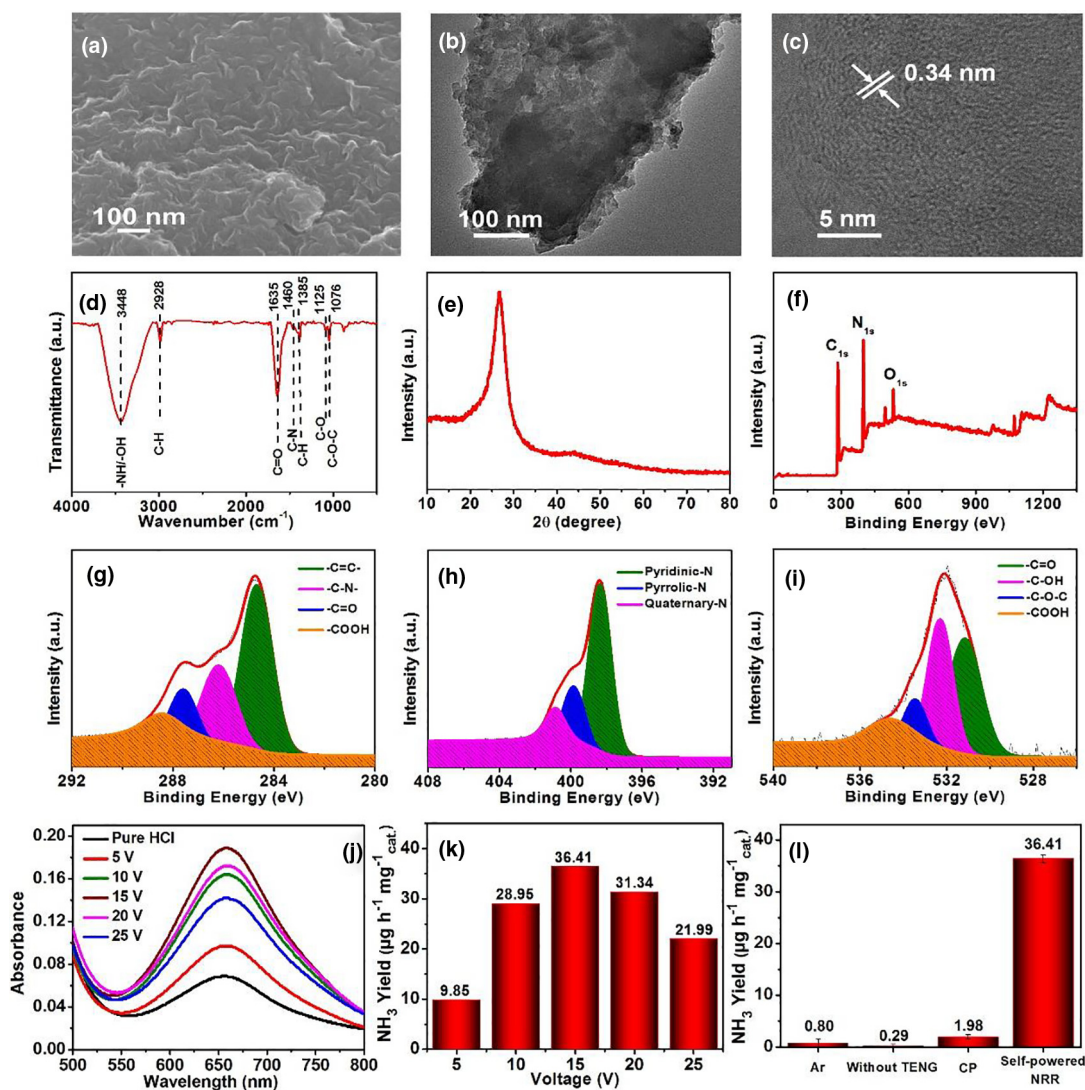


FIGURE 3

(a) Basic structure and fabrication process of the PMLA-TENG. (b) The potential distribution simulated by COMSOL with the angle changes. (c)  $I_{sc}$ , (d)  $Q_{tr}$ , and (e)  $V_{oc}$  of the PMLA-TENG with different pair of friction layers. The  $V_{oc}$  of the PMLA-TENG with six friction layers is inserted in (e). (f) The instantaneous current and the power density of the PMLA-TENG with six friction layers as the load resistance increases. (g)  $I_{sc}$  after processed by a transformer and a rectifier. (h) The  $I_{sc}$  processed by a transformer and a rectifier after about 136,800 cycles, (working continuously for 6 h).

them as promising power sources *via* harvesting mechanical energy from various ambient environment. Here, PMLA-TENG was selected as an example to be successfully assembled into self-powered electro-Fenton degradation device and self-powered electrochemical polymerization system (shown in [supporting information, Figs. S4 and S5](#)), which greatly encourages us to integrate the 3D printed PMLA-TENG as a power supply with electrocatalytic N<sub>2</sub> reduction system. Here, MSCM with high nitrogen content, abundant 2D layered structure and good conductivity were obtained *via* high temperature pyrolysis and utilized as the electrocatalyst. Its SEM, TEM, XRD, FTIR and XPS characterizations ([Fig. 4a–i](#)) are described in details in [Supporting Information](#). The electrocatalytic NRR tests driven by PMLA-TENG are performed as shown in experimental section. To demonstrate the effective N<sub>2</sub> electroreduction in 0.1 mol L<sup>-1</sup> HCl, the production of both NH<sub>3</sub> and a possible by-product hydrazine (N<sub>2</sub>H<sub>4</sub>) are spectrophotometrically estimated after 2 h electrolysis operation by the indophenol blue method and

the method of Watt and Chrisp<sup>4</sup>, respectively (the corresponding calibration curves are shown in [supporting information Figs. S6–7](#)). [Fig. 4j](#) shows the UV–vis absorption spectra of the indophenol-indicator-colored electrolyte produced by PMLA-TENG-powered NRR in the voltage range from 5 to 25 V. The calculated NH<sub>3</sub> yields are shown in [Fig. 4k](#) with the peak of 36.41 μg h<sup>-1</sup> mg<sup>-1</sup> cat. when the rectified instantaneous maximum voltage between two electrodes of the nitrogen fixation reactor is about 15 V, demonstrating that PMLA-TENG can facilitate the reduction of N<sub>2</sub> to NH<sub>3</sub> using MSCM as the cathode materials. To confirm that the generated NH<sub>3</sub> molecules mainly stem from the electrocatalyzed conversion of N<sub>2</sub> by the self-powered N<sub>2</sub> electroreduction system, a series of control experiments were performed with an Ar-saturated electrolyte, without additional power source applied to the electrodes under N<sub>2</sub> gas and bare CP without catalyst. The corresponding UV–vis absorption spectra ([Fig. S8](#)) and calculated NH<sub>3</sub> yields ([Fig. 4l](#)) reveal the existence of a small amount of NH<sub>3</sub> that may originate from sources of



**FIGURE 4**

(a) FESEM, (b) TEM (c) HR-TEM, (d) FT-IR, (e) XRD (f) full-scan XPS spectrum, and high-resolution XPS spectra of C 1s (g), N 1s (h), O 1s (i) of MSCM. (j) Corresponding UV–vis absorption spectra of the indophenol-indicator-colored electrolyte produced by PMLA-TENG-powered NRR in the voltage range from 5 to 25 V. (k) NH<sub>3</sub> yield rate at different voltage. (l) NH<sub>3</sub> yield rate under various conditions after electrolysis for 2 h.

contamination (e.g., laboratory, device, membrane). Obviously,  $N_2H_4$  was not detected, confirming that this self-powered  $N_2$  electroreduction system possesses excellent selectivity for  $NH_3$  formation (Fig. S9). The above results revealing that (1) the PMLA-TENG is powerful enough to drive electroreduction of  $N_2$  and (2) the MSCM is highly active to catalyze  $N_2$  electroreduction.

## Conclusions

An integration of 3D printing technology with fabrication of TENGs provides a new strategy to design and tailor TENGs with complex 3D geometries, which can make TENGs with high performance and complex personalized structure for achieving scalable 3D fabrication, eventually greatly broadening the application scope in flexible and potable self-powered systems. The self-powered  $N_2$  fixation system via integrating PMLA-TENG featuring a maximum power density of  $6.7 \text{ W m}^{-2}$  as power supply with the carbon materials from MS as the metal-free electrocatalyst to efficiently drive  $N_2$  reduction into  $NH_3$ , which represents a pioneering step toward perfect marriage of the digital manufacturing of TENGs by 3D printing with self-powered sustainable fixation methods for  $NH_3$  from  $N_2$  under ambient conditions.

## Acknowledgments

This work was supported by the National Natural Science Foundation of China, China (Grant Nos. 51872076 and U1804255), the Program for Innovative Research Team of Henan Scientific Committee (CXTD2014033) and the Project of Central Plains Science and Technology Innovation Leading Talents, Henan Province (Grant No. 194200510001).

## Appendix A. Supplementary data

Supplementary data to this article can be found online at <https://doi.org/10.1016/j.mattod.2019.05.004>.

## References

- [1] R.F. Service, *Science* 345 (2014) 610.
- [2] J. Li et al., *Acc. Chem. Res.* 50 (2017) 112–121.
- [3] C. Guo et al., *Energy Environ. Sci.* 11 (2018) 45–56.
- [4] X. Cui, C. Tang, Q. Zhang, *Adv. Energy Mater.* 8 (2018) 1800369.
- [5] L. Wang et al., *Joule* 2 (2018) 1055–1074.
- [6] L. Zhang et al., *Adv. Mater.* 30 (2018) 1800191.
- [7] H.K. Lee et al., *Sci. Adv.* 4 (2018) eaar3208.
- [8] Y. Liu et al., *ACS Catal.* 8 (2018) 1186–1191.
- [9] H. Cheng et al., *Adv. Mater.* 30 (2018) 1803694.
- [10] Z. Geng et al., *Adv. Mater.* 30 (2018) 1803498.
- [11] C. Lv et al., *Angew. Chem. Int. Ed.* 130 (2018) 6181–6184.
- [12] W. Qiu et al., *Nat. Commun.* 9 (2018) 3485.
- [13] Q. Hua et al., *Nat. Commun.* 9 (2018) 244.
- [14] Y. Yang et al., *Chem. Commun.* 53 (2017) 9994–9997.
- [15] X. Cao et al., *Adv. Mater.* 30 (2018) 1704077.
- [16] H. Guo et al., *ACS Nano* 11 (2017) 4475–4482.
- [17] J. Wang et al., *Adv. Func. Mater.* 26 (2016) 3542–3548.
- [18] B. Chen, Y. Yang, Z.L. Wang, *Adv. Energy Mater.* 8 (2018) 1702649.
- [19] Y. Chen et al., *Nano Energy* 50 (2018) 441–447.
- [20] X. Wang et al., *ACS Nano* 11 (2017) 1728–1735.
- [21] Z.-H. Lin et al., *Angew. Chem. Int. Ed.* 125 (2013) 12777–12781.
- [22] B.D. Chen et al., *Mater. Today* 21 (2018) 88–97.
- [23] Z. Li et al., *Adv. Mater.* 28 (2016) 2983–2991.
- [24] Z.-H. Lin et al., *Adv. Mater.* 26 (2014) 4690–4696.
- [25] F. Yi et al., *ACS Nano* 10 (2016) 6519–6525.
- [26] Z.L. Wang, *Nature* 542 (2017) 159–160.
- [27] L. Xu et al., *ACS Nano* 12 (2018) 1849–1858.
- [28] U. Khan, S.-W. Kim, *ACS Nano* 10 (2016) 6429–6432.
- [29] B. Derby, *Science* 338 (2012) 921–926.
- [30] M. Montgomery et al., *Nat. Mater.* 16 (2017) 1038–1046.
- [31] M. Scholze et al., *Sci. Rep.* 8 (2018) 11340.
- [32] M. Wehner et al., *Nature* 536 (2016) 451–455.
- [33] N.W. Bartlett et al., *J. Science* 349 (2015) 161–165.
- [34] D.K. Patel et al., *Adv. Mater.* 29 (2017) 1606000.
- [35] J. Morrow, S. Hemleben, Y. Menguc, *IEEE Robotics Autom. Lett.* 2 (2017) 277–281.
- [36] T. Gissibl et al., *Nat. Photonics* 10 (2016) 554–560.
- [37] X. Chen et al., *Adv. Mater.* 30 (2018) 1705683.
- [38] H. Yang et al., *Adv. Mater.* 29 (2017) 1701627.
- [39] M. Zarek et al., *Adv. Mater.* 28 (2016) 4449–4454.
- [40] C. Wu et al., *Mater. Today* 21 (2018) 216–222.
- [41] J. Lu et al., *Mater. Today* 24 (2019) 33–40.
- [42] S.-F. Leung et al., *Energy Environ. Sci.* 7 (2014) 3611–3616.
- [43] K. Fu et al., *Adv. Mater.* 28 (2016) 2587–2594.
- [44] K. Fu et al., *Adv. Mater.* 29 (2017) 1603486.
- [45] Y. Lin et al., *Nano Res.* 11 (2018) 3065–3087.
- [46] T.J. Wallin, J. Pikul, R.F. Shepherd, *Nat. Rev. Mater.* 3 (2018) 84–100.
- [47] Y. Jiang, Q. Wang, *Sci. Rep.* 6 (2016) 34147.
- [48] S. Niu et al., *Energy Environ. Sci.* 6 (2013) 3576–3583.
- [49] S. Gao et al., *ACS Nano* 11 (2017) 3965–3972.
- [50] R.E. Drumright, P.R. Gruber, D.E. Henton, *Adv. Mater.* 12 (2000) 1841–1846.
- [51] S. Bose, S. Vahabzadeh, A. Bandyopadhyay, *Mater. Today* 16 (2013) 496–504.